Journal of Membrane Science 678 (2023) 121689

Contents lists available at ScienceDirect

Journal of Membrane Science

journal homepage: www.elsevier.com/locate/memsci

Engineering highly permeable thin-film composite nanofiltration membranes by strengthening the diffusion control of amine monomer via deep eutectic solvent

Yao Fang [a,1], Bin Jiang [a,1], Yufan Hao [a], Na Yang [a], Longfei Zhang [b], Congcong Zhang [a], Yongli Sun [a], Xiaoming Xiao [a], Luhong Zhang [a,*]

[a] School of Chemical Engineering and Technology, Tianjin University, Tianjin, 300072, China
[b] School of Chemistry and Chemical Engineering, Tianjin University of Technology, Tianjin, 300384, China

ARTICLE INFO

Keywords:
Deep eutectic solvent
Polyamide
Interfacial polymerization
Nanofiltration

ABSTRACT

Thin-film composite nanofiltration (TFC NF) membranes play an important role in seawater desalination and wastewater decontamination, while the presence of trade-off effect between permeability and selectivity limits their further application. Tuning amine monomer diffusion has been considered as the key to optimizing the physicochemical structure of polyamide (PA) layer and thus achieving the preparation of highly permeable TFC NF membranes. In this study, deep eutectic solvent (DES) was used as an aqueous-phase additive to enhance the control of piperazine (PIP) diffusion via a novel integrated synergistic mechanism of hydrogen bonding interaction and viscosity modulation during interfacial polymerization (IP) process. Correspondingly, the addition of DES can not only optimize membranes surface properties (hydrophilicity, surface negative charge, roughness) but also reduce the thickness of PA layer from 93 ± 9 nm to 31 ± 4 nm. The results showed that the modified membrane maintained a high Na_2SO_4 rejection (99.3%) and a favorable pure water permeance of 43.3 $L{\cdot}m^{-2}{\cdot}h^{-1}{\cdot}bar^{-1}$, which presented approximately 6-fold higher pure water permeance than that of commercial membranes NF-90. Therefore, this study provides a promising strategy to fabricate highly permeable TFC NF membranes and opens up a new avenue for DES application in water treatment.

1. Introduction

Owing to the rapid world population growth and increasing industrialization, water pollution and shortage have become one of the most serious challenges worldwide [1,2]. Membrane separation technology, as an efficient and environmentally friendly water treatment technology, draws extensive attention in dealing with the prevailing water crisis [3–6]. In recent decades, polyamide (PA) membranes fabricated via interfacial polymerization (IP) and their derived thin-film composite nanofiltration (TFC NF) membranes have become prevalent among the membrane markets for water processing [7]. During the typical IP process, the PA separation layer is manufactured on the substrate through cross-linking process occurred between amine monomers and acyl chloride monomers, which mainly dominates the permeability and selectivity of TFC NF membranes [8–10]. However, the presence of trade-off effect between permeability and selectivity limits the further development and application of TFC NF membranes [11]. Therefore, regulating the properties of PA separation layer could be promising in decreasing the limitation of the trade-off effect and augmenting permeability as much as possible while maintaining selectivity [12].

It is generally believed that IP reaction is a typical reaction-diffusion process far from thermodynamic equilibrium [13]. To date, most studies have agreed that the amine monomers diffuse and cross the water-oil phase interface for polymerization reaction with acyl chloride monomers in the organic phase [14,15]. But this reaction procedure is extremely fast and uncontrollable, which can quickly generate a dense PA layer with tens or even hundreds of nanometers thick, resulting in NF membranes normally with poor permeability [16,17]. Therefore, tuning the diffusion rate of amine monomers into the organic phase is crucial for regulating the properties of PA separation layer with desirable structure and enhanced performance [18].

Until now, adding additives in aqueous phase solution is considered

* Corresponding author. School of Chemical Engineering and Technology, Tianjin University, Tianjin, 300072, China.
E-mail address: zhanglvh@tju.edu.cn (L. Zhang).
[1] These authors contribute equally to this work.

https://doi.org/10.1016/j.memsci.2023.121689
Received 12 February 2023; Received in revised form 31 March 2023; Accepted 20 April 2023
Available online 21 April 2023

as a simple method. Recently, numerous rigid nanomaterials, such as TiO_2 [19], MWNT [20], GO [21], have been extensively investigated and reported as aqueous-phase additives. However, the rigid nanomaterials themselves are easy to aggregate and have poor compatibility with the PA layer, leading to the poor mechanical stability of NF membranes [22–24]. In contrast, some organic molecules can act as a mild and effective aqueous-phase additive to inhibit amine monomers diffusion through single interaction. Meanwhile, they can be easily washed off by deionized water after IP reaction, avoiding the risk of additive spillage in the separation process [25–27]. For example, Zhang et al. used phytic acid dodecasodium salt (PADS) to retard PIP diffusion through electrostatic interaction. The obtained NF membranes presented a 21.24 $L{\cdot}m^{-2}{\cdot}h^{-1}{\cdot}bar^{-1}$ of water permeance and a 97.35% of Na_2SO_4 rejection [28]. In addition to controlling PIP diffusion by single interaction, the multi-action regulation of PIP diffusion has also been successfully applied, and the prepared PA membranes exhibit good NF performance [13,25,29]. For instance, Li et al. used GQDs as aqueous phase additive to inhibit the diffusion rate of PIP through chemical affinity (hydrogen bonding, electrostatic interaction) and steric hindrance [30]. The pure water permeance and Na_2SO_4 rejection of obtained PA nanofilms were 32.1 $L{\cdot}m^{-2}{\cdot}h^{-1}{\cdot}bar^{-1}$ and 99.6%, respectively. Therefore, it is a simple and feasible strategy to enhance NF performance by exploring more additives that can multi-action regulate PIP diffusion. Meanwhile, the mechanism to strengthen the control of PIP diffusion is worth investigating.

Deep eutectic solvents (DESs), known as cheap and green alternatives for ionic liquids (ILs), attract extensive attention [31]. They are usually prepared by certain molar ratios of hydrogen bond donors (HBD) and hydrogen bond acceptors (HBA), where extensive hydrogen bonding interaction is the driving force to form eutectic mixtures [32,33]. Recently, DESs have been widely used in gas absorption [34,35], nanomaterials synthesis [36], catalysis [37], organic synthesis [38] and other fields because of their universal dissolution abilities, easily prepared, high viscosity and multi-task applicability [39,40]. However, the application of DESs in the field of TFC membranes is limited to the surface cleaning and modifying agents for the reverse osmosis (RO) membranes [41,42]. For example, Mondal et al. treated the surface of pristine PA membrane with DESs, and the obtained membranes with improved surface wettability and high flux recovery [43]. To date, the use of DESs as aqueous-phase additives for synthesizing NF membranes has not been reported.

Herein, a water-soluble and biocompatible as well as widely applied choline chloride-ethylene glycol based DES, was used as the aqueous-phase additive to strengthen the diffusion control of PIP for synthesizing highly permeable TFC NF membranes. The DES can interact with PIP in the form of hydrogen bonding [44], and its high viscosity feature can change the viscosity of aqueous phase solution. Besides, it is cheaper, easier to prepare and more biodegradable than other additives such as hydrophilic macromolecules, acid organic acids and porous organic polymers [41,45]. Based on these properties, the effect of DES addition on the PIP diffusion rate was systematically studied by viscosity measurement and theoretical analysis as well as diffusion experiments. Moreover, the properties variation of PA separation layer resulting from DES addition was analyzed in detail. In addition, the separation performance of TFC NF membranes was evaluated via changing DES concentration in aqueous phase solution. Furthermore, the operation stability and antifouling properties of the obtained TFC NF membranes for this experiment were also evaluated.

2. Experimental

2.1. Chemicals and materials

Commercial Polyethersulfone microporous membranes (PES, pore diameter: 220 nm) were supplied by Haiyan Xindongfang Suhua Co., Ltd. Trimesoyl chloride (TMC, 98%) was obtained by Shanghai Macklin Biochemical Technology Co., Ltd. Piperazine (PIP, 99%, AR) was supplied by Aladdin Chemical Co., Ltd. Choline chloride (ChoCl ，98%) and Bovine serum albumin (BSA, 98%, AR) were provided by Tianjin Heowns Opde Technology Co., Ltd. Polyethylene glycols (PEG, 200, 400, 600, 800 and 1000 Da) were provided from Sinopharm Chemical Reagent Co., Ltd. Inorganic salts (Na_2SO_4, $MgSO_4{\cdot}7H_2O$, NaCl and $MgCl_2{\cdot}6H_2O$, AR), ethylene glycol (AR) and *n*-hexane (AR) were supplied by Tianjin Kemiou Chemical Reagent Co., Ltd. Deionized (DI) water was utilized during the experiment.

2.2. Preparation of choline chloride-ethylene glycol based DES (ChoCl-EG)

The DES was prepared in following manner according to the literature [46]. Typically, ethylene glycol and choline chloride in molar ratio of 2:1 were poured into 200 mL glass container and keep it for stirring at 60 °C until a clear homogenous solution was available. Afterwards, the solution was dried under vacuum condition at 60 °C for about 24 h to remove any water that may be present.

2.3. Fabrication of TFC membranes

Fig. 1 showed the synthesis process of TFC-X membranes. The 0.2 wt % of PIP was dissolved in aqueous phase solution with different DES concentrations. The 0.15 wt% of TMC was dissolved in *n*-hexane. The IP process was conducted in a vacuum filtration device with a 12.56 cm^2 effective area. Firstly, PES microfiltration membranes were fixed in the device, and 3 mL PIP solution was added onto the membranes surface. After 8 min, the remaining PIP solution was removed under −0.1 MPa pressure. After that, adding 3 mL TMC solution onto the membranes surface and the reaction proceeded for 1 min. Then, removing the residual TMC solution, the nascent membranes were post-treatment for 20 min at 60 °C. Finally, the prepared NF membranes were transferred to DI water before testing. The membranes prepared by the above method were noted as TFC-X, in which X means the DES concentration in aqueous phase solution.

2.4. Membranes characterization

The surface and cross-sectional morphologies were characterized through scanning electron microscopy (SEM, Hitachi, Regulus 8100, Japan). The transmission electron microscope (TEM, JEM-1400Flash, Japan) was used to characterize the cross-sectional morphologies of TFC-X membranes treated by ultrathin section specimens. The atomic force microscopy (AFM, Bruker, Dimension icon, Germany) was utilized to evaluate the roughness of membranes surface. The membranes surface charge was measured at the pH about 7 using an electrokinetic analyzer (Surpass, Anton Paar, Austria). The attenuated total reflectance Fourier transform infrared spectroscopy (ATR-FTIR, Thermo Scientific Nicolet iS20, USA) and X-ray photoelectron spectra (XPS, Thermo

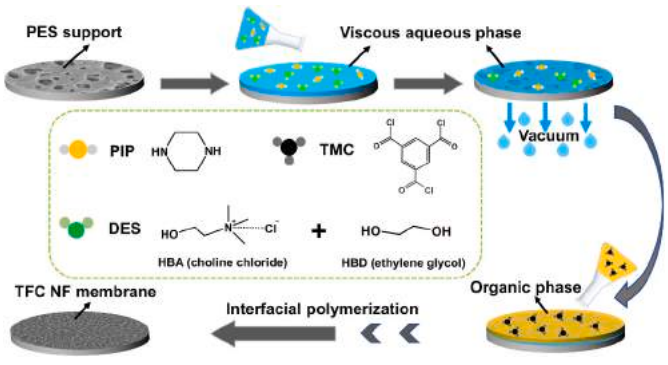

Fig. 1. Schematic illustration of the synthesis process of TFC-X membranes.

Scientific K-Alpha, USA) were taken to investigate the chemistry structure of membranes surface. The water contact angle (WCA) of membranes surface was measured using a goniometer (Powereach, JC 2000). Each membrane sample was measured three times at randomly selected locations and averaged.

2.5. Separation performance of TFC membranes

The separation experiments were carried out via a cross-flow filtration device with a 7.07 cm^2 effective filtration area. Prior to testing, the membranes were prepressed with DI water at 5 bar for 30 min, and then remained stable at 4 bar for 10 min. The separation experiments were carried out using different salt solutions (Na_2SO_4, $MgSO_4$, $MgCl_2$ and NaCl) with 1000 ppm concentration at 4 bar. The pure water flux (F, $L{\cdot}m^{-2}{\cdot}h^{-1}$) was obtained by Eq. (1):

$$F = (\Delta V)/(A \bullet \Delta t) \tag{1}$$

where ΔV corresponds to the volume of permeate (L), A corresponds to the effective membrane area (m^2) and Δt corresponds to the testing time (h).

The permeance (P, $L{\cdot}m^{-2}{\cdot}h^{-1}{\cdot}bar^{-1}$) was determined based on Eq. (2):

$$P = F/\Delta P \tag{2}$$

where ΔP corresponds to the operating pressure.

Salt rejection was obtained from Eq. (3):

$$R = \left(1 - C_P/C_f\right) \times 100\% \tag{3}$$

where C_P and C_f correspond to the salt concentration of the permeate and feed solutions, respectively, which can be detected by a conductivity monitor (Leici, DDS-307A, China).

2.6. Antifouling properties evaluation

The antifouling experiment of TFC-X membranes was conducted via a cross-flow filtration device with bovine serum albumin (BSA) as pollutants. In addition, by adjusting the operating pressure so that the pure water fluxes of membranes remained consistent, ensuring the TFC-X membranes could be tested under identical lateral hydrodynamic properties [6,47]. Firstly, the pure water was filtrated for 2 h at 4 bar. Secondly, the pure water was replaced with BSA solution for another 2 h. Next, rinsing contaminants from the membranes with pure water without applying pressure. The flux recovery ratio (FRR) was computed using Eq. (4) [48]:

$$FRR(\%) = \frac{J_w}{J_0} \times 100\% \tag{4}$$

where J_0 represents the initial flux and J_w represents the water flux after washing, respectively.

2.7. Diffusion experiment of PIP from aqueous phase to organic phase

For this experiment, the concentration of PIP was chosen to be 1 wt% in order to amplify the effect of DES addition on the PIP diffusion. Firstly, the PIP solution with different concentrations of DES was added to a 50 mL sample bottle, and then 10 mL of *n*-hexane was slowly injected above the aqueous phase solution with a pipette. After diffusion for 1 min, 3 mL of the *n*-hexane solution containing PIP was removed from the *n*-hexane-air interface and added into cuvettes. The UV–vis spectrometer (UV–4802S, Unico, US) was used to monitor the absorbance of PIP in *n*-hexane. The PIP shows a typical absorption peak at about 220 nm, and peak intensity indicates the PIP concentration in *n*-hexane [49].

3. Results and discussion

3.1. Effect of DES on PIP diffusion

Choline chloride-ethylene glycol based DES, with a viscosity of about 37 times that of water at room temperature, and can be miscible with water in any proportion [50]. In our experiment, the viscosity of aqueous phase solution was measured with a viscometer (Brookfield DV-II + Pro) at 303.15 K (Fig. 2a), which increased continuously from 0.91 mPa·s to 13.21 mPa·s with increasing DES concentration (0–90 wt %). In addition, the interaction between DES and PIP was analyzed via density-functional theory (DFT) calculations using Gaussian 09 program at B3LYP/6–311++G(d,p) level of theory [51,52]. As shown in Fig. 2b, there is strong hydrogen bonding interaction between PIP and DES, including N–H···Cl^-, OH···N–H and N–H···(–CH_3)C–H, which verifies that PIP can also participate in the hydrogen bonding network of DES as HBD. In order to explore the impact of DES introduction on the PIP diffusion behavior, we conducted the interfacial diffusion experiment. As illustrated in Fig. 2c, the intensity of the PIP adsorption peak decreased continuously as the DES concentration gradually increased. This represents the DES addition is able to inhibit the diffusion rate of PIP via hydrogen bonding between DES and PIP as well as increased solution viscosity. Besides, the inhibition of PIP diffusion became more apparent with the increase of DES concentration, which is beneficial to construct thinner PA layer based on the Freger equation [53,54].

3.2. Structural characterization of membranes

The ATR-FTIR was applied to investigate the surface chemical structure of the membranes (Fig. 2d). Compared with the PES support, the TFC-X membranes showed a new peak at 1625 cm^{-1}, which corresponded to the C═O stretching vibration of amide group (–CO–NH-), proving that the IP reaction occurred successfully on the TFC-X membranes [55]. Meanwhile, there was no distinguishable peaks around 1725 cm^{-1}, which excluded the possibility of "acyl-hydroxyl" esterification between DES and TMC during IP process. These results show that the introduction of DES only affects the PIP diffusion rate with no influence on the composition of the separated layer [56,57].

In order to investigate the changes in the surface chemistry of membranes after DES addition, the XPS spectroscopy was utilized to analyze the elemental compositions of TFC-X membranes. Table 1 showed the C, N, O element content and the cross-linking degree of TFC-X membranes calculated from the element content ratios of N to O (**Note S1**) [10]. The cross-linking degree of TFC-X membranes gradually decreased from 84.39% to 69.28% with increasing DES concentration (0–90 wt%). To further study the effect of DES addition on the functional groups content of membranes surface, the convolution spectra analysis of C1s, O1s and N1s is presented in Fig. S1 and Table S1. The content of both O–C═O groups and N–H groups on the surface of TFC membranes increased with the increase of DES concentration, which again verified a decrease in the cross-link degree of TFC-X membranes [18,58]. The above phenomenon can be attributed to the following aspects: After adding DES into the aqueous phase solution, the PIP diffusion rate was suppressed, resulting in less PIP crossing the water-oil phase interface to participate in the IP reaction with TMC. Consequently, more of the chloride groups in TMC hydrolyzed and formed carboxylic acids rather than cross-linked by the PIP.

The surface morphology of membranes was characterized by SEM and AFM. The nodular structure appeared on the TFC-0 membrane surface compared to the PES substrate (Fig. 3a and b), which is a typical PA surface fabricated by cross-linking reaction between TMC and PIP [59]. With the increase in DES addition, the nodular structure of TFC-X membranes surface declined and finally disappeared when increasing DES concentration to 90 wt%. Interestingly, the cellular-like structure was observed on the TFC-60% membrane surface. The above changes of membranes surface morphology can be illustrated by Fig. 3e. Through

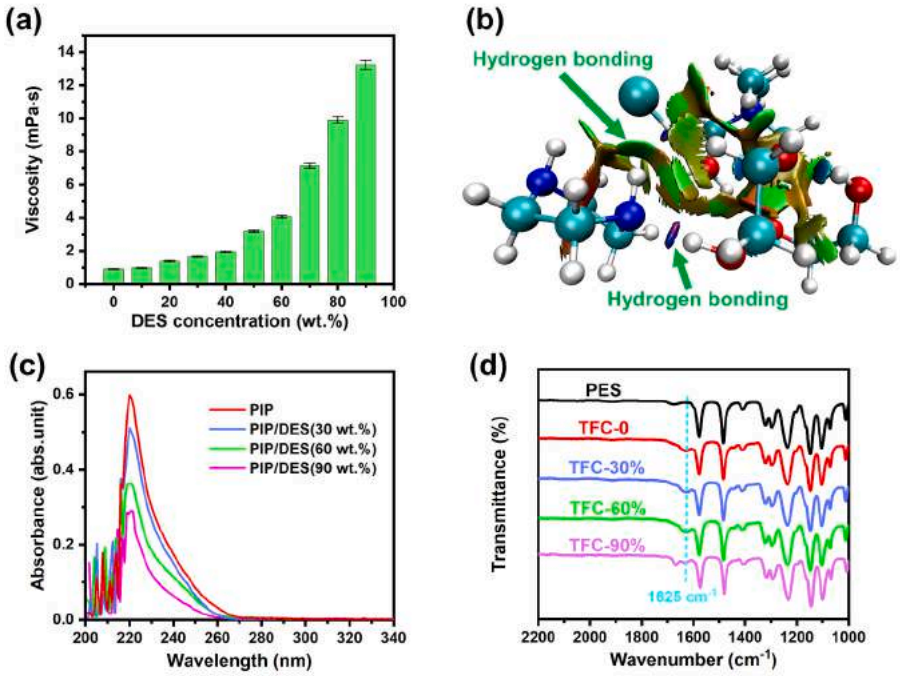

Fig. 2. (a) Effect of DES on the viscosity of the aqueous solution. (b) The interaction between DES and PIP by density-functional theory (DFT) calculations. (c) UV–vis spectra of PIP in the organic phase after 1 min of diffusion. (d) The ATR-FTIR spectra of PES and TFC-X membranes.

Table 1
Atomic composition and cross-linking degree of the TFC-X membranes.

Sample	Atomic composition (%)			N/O molar ratio	Cross-linking degree (%)
	C	N	O		
TFC-0	73.17	11.31	15.52	0.73	84.39
TFC-30%	72.66	10.74	16.60	0.65	78.78
TFC-60%	71.85	10.48	17.67	0.59	74.21
TFC-90%	71.23	9.81	18.46	0.53	69.28

the vacuum-assisted method, the aqueous phase solution was closely adhered to the PES substrate (Fig. 3e1) [60]. When the IP reaction occurred on this basis, the PA layer generated by the aqueous phase solution without DES was shown in Fig. 3e2. The thick PA layer and the stacked PA inside the membrane pores caused the increased resistance to water molecule transport. With the increase of DES concentration (0–90 wt%), the inhibition of PIP diffusion becomes apparent, the PES substrate gradually plays an important role in affecting the surface morphology of PA separation layer [57,61,62]. As illustrated in Fig. 3e3, the cellular-like structure of TFC-60% membrane is similar to that of the PES substrate, which is associated with the thin thickness of PA separation layer [49,62]. When the DES concentration increased to 90 wt%, the aqueous phase solution viscosity increased and the hydrogen bonding interaction between DES and PIP enhanced. Consequently, the PIP diffusion rate was dramatically decreased and that the IP reaction was incomplete, resulting in the complete disappearance of the nodular structure on the generated PA layer [25].

From AFM images presented in Fig. 3c, it can also be found that the surface morphology of TFC-X membranes is similar to the SEM images (Fig. 3a and b). When the DES concentration is 30 wt%, the PIP diffusion was inhibited, leading to a little decline in nodular structure on the surface of TFC-30% membrane compared to TFC-0 membrane, and a slight decrease in the average surface roughness (Ra) from 33.7 nm to 29.9 nm [28]. As the DES concentration increases to 60 wt%, the TFC-60% membrane surface showed the cellular-like structure, and the corresponding Ra increased to 40.9 nm, which was derived from the simultaneous presence of nodular structure and replicated PES substrate morphology [62]. When the concentration of DES is 90 wt%, the PIP diffusion was significantly inhibited and the nodular structure disappeared, resulting in a smooth membrane surface with Ra only 23.6 nm, despite the fact that TFC-90% membrane surface replicated PES substrate morphology. In addition, the relative surface area increments of TFC membranes obtained from AFM images are listed in Table S2, indicating that the cellular-like structure can significantly enhance the specific surface area of TFC-60% membrane [61]. The PA layer thickness of TFC-X membranes was also influenced by the addition of DES. Fig. 3d shows that the PA layer thickness measured by SEM gradually decreased from 93 ± 9 nm to 31 ± 4 nm with increasing DES concentration from 0 to 90 wt%. Meanwhile, the thickness of PA layer was also measured by TEM in Fig. S2, which decreased from 85 ± 7 nm to 26 ± 3 nm as the DES concentration increased (0–90 wt%). Both SEM and TEM results show a similar change trend in the thickness of PA layers after DES addition. As mentioned before, we have demonstrated that the higher the DES concentration in aqueous phase solution, the more obvious the inhibition of PIP diffusion rate. Therefore, a thinner PA layer will be generated as the DES concentration increases based on the Freger equation.

The hydrophilicity and surface potential of TFC-X membranes were displayed in Fig. 4a and b. The water contact angle (WCA) of TFC-X membranes decreased as DES addition increased, suggesting that there was a significant enhancement of hydrophilicity on TFC-X membranes surface [63]. The surface charged property of TFC-X membranes decreased from −42.5 mV to −46.6 mV when the DES adding dosage increased from 0 to 90 wt%. This enhanced negatively charged property is expected to strengthen the repellency to divalent anions [10,64]. The enhancement of hydrophilicity and negative charge of TFC-X membranes was because of the increased carboxyl groups generated from the hydrolysis of uncross-linked chloride groups in TMC. This corresponded to the surface chemical properties of PA separation layer analyzed before.

The pore size of TFC-X membranes significantly affects their

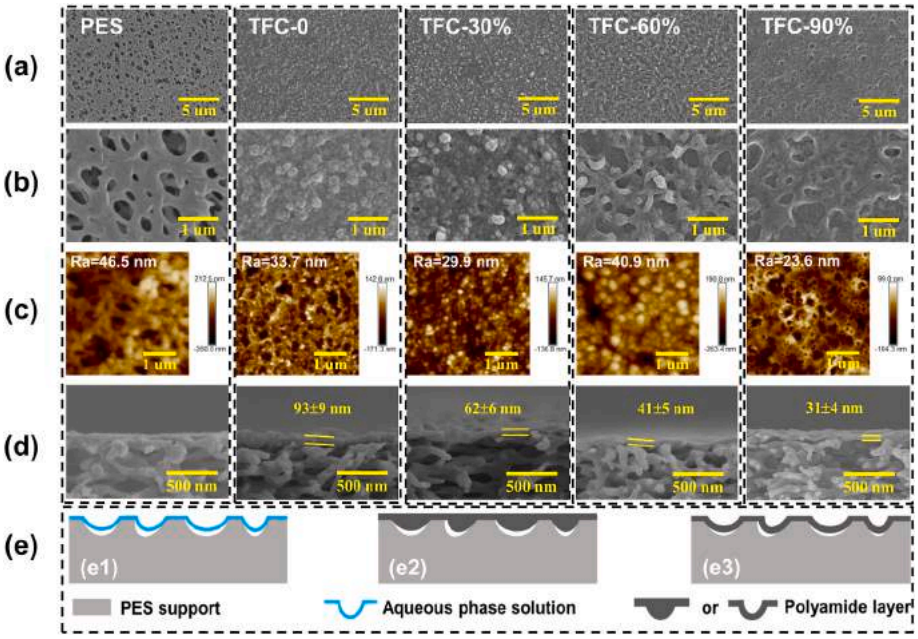

Fig. 3. SEM (a–b) and AFM (c) surface morphology of the PES and TFC-X membranes. SEM cross-sectional morphology of the PES and TFC-X membranes (d). The structural models of PES membrane containing aqueous phase solution (e1), TFC-0 membrane (e2) and TFC-60% membrane (e3).

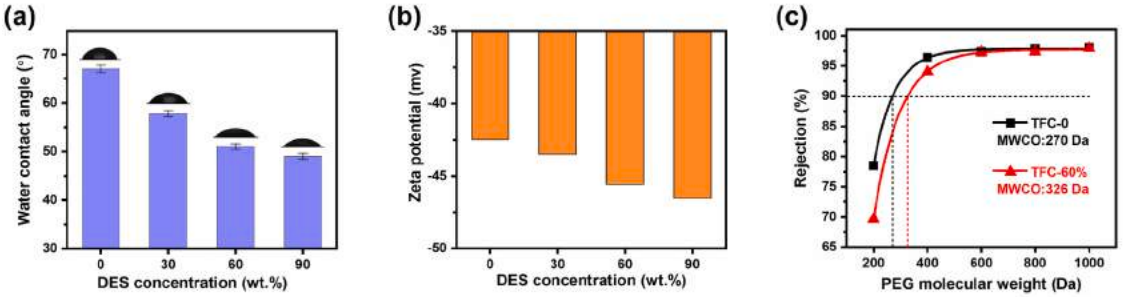

Fig. 4. (a) Static water contact angles. (b) Surface zeta potential (pH = 7). (c) Rejection curves to PEG with different molecular weight.

separation performance. We used a range of neutral polyethylene glycol (PEG) at various molecular weights (200–1000 Da) to evaluate the neutral molecules rejection and molecular weight cut-off (MWCO) of TFC-X membranes [65]. As illustrated in Fig. 4c, both TFC-0% membrane and TFC-60% membrane show a high rejection over 97% for neutral PEG with molecular weights above 600 Da. Meanwhile, the MWCO of TFC-60% membrane increased to 326 Da compared to the TFC-0 membrane (270 Da), indicating that the DES addition is beneficial to form a relatively loose PA layer [66].

3.3. Separation performance of TFC-X membranes

The separation performance of TFC-X membranes was investigated by testing the pure water permeance and Na_2SO_4 rejection rate. As seen in Fig. 5a, the introduction of DES significantly improved the pure water permeance of TFC-X membranes. Especially, when the DES concentration was 60 wt%, there was a sharp increase in the pure water permeance. Among them, the pure water permeance of TFC-60% membrane was 43.3 $L{\cdot}m^{-2}{\cdot}h^{-1}{\cdot}bar^{-1}$, increased by 143% compared with 17.8 $L{\cdot}m^{-2}{\cdot}h^{-1}{\cdot}bar^{-1}$ of TFC-0 membrane, while the Na_2SO_4

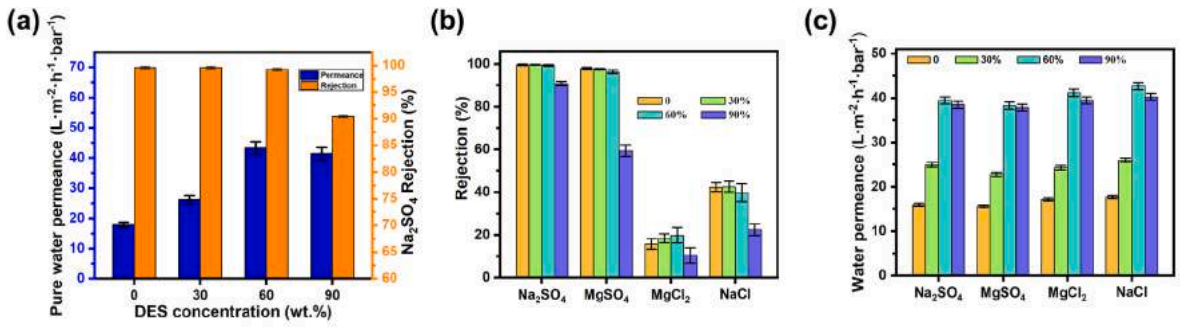

Fig. 5. (a) The pure water permeance and Na_2SO_4 rejection of TFC-X membranes. (b–c) Salt rejection and water permeance of TFC-X membranes.

rejection remained 99.3%, showing excellent separation performance. This could be ascribed to the three factors as follows: Firstly, the thickness of PA separation layer in TFC-60% membrane was only 41 ± 5 nm, which shortens the transport pathway and reduces the transport resistance of water [67]. Secondly, owing to the increased carboxyl groups on membrane surface, the surface negative charge and hydrophilicity are enhanced, which facilitates water molecule transfer as well as maintains a high rejection for Na_2SO_4 [68]. Thirdly, the relatively loose structure and the high relative surface area increments accelerate the transport of water molecules [61]. When the concentration of DES was 90 wt%, an ultrathin but defective PA layer was generated and the rejection rate of Na_2SO_4 was only 90.4%. Meanwhile, the lower relative surface area increments of TFC-90% membrane results in a slight decrease of its pure water permeance from 43.3 $L{\cdot}m^{-2}{\cdot}h^{-1}{\cdot}bar^{-1}$ to 41.4 $L{\cdot}m^{-2}{\cdot}h^{-1}{\cdot}bar^{-1}$. Thus, the optimal DES concentration was 60 wt%, where the TFC-60% membrane performed best with a 43.3 $L{\cdot}m^{-2}{\cdot}h^{-1}{\cdot}bar^{-1}$ of pure water permeance and a 99.3% of Na_2SO_4 rejection. In addition, the relationship between PIP concentration and TFC membranes separation performance at a DES concentration of 60 wt % was studied in detail (**Note S2,** Fig. S3 **and** Fig. S4**).**

Fig. 5b and c displays the salt rejection and water permeance of TFC-X membranes for different inorganic salts solution. The sequence of salt rejection is: $Na_2SO_4 > MgSO_4 > NaCl > MgCl_2$, determined by the size sieving and the Donnan effect [63,69]. The detail explanation is as follows: Due to the negatively charged TFC-X membranes surface, the repellency of SO_4^{2-} is stronger than that of Cl^-, making the $MgSO_4$ rejection is higher than that of $MgCl_2$. However, the presence of negative charge weakens the repellency of TFC-X membranes for Mg^{2+}, resulting in the lowest rejection of $MgCl_2$, indicating that the dominance of the Donnan effect in this process [70]. Meanwhile, this is why TFC-60% membrane with more negative charge maintains a high Na_2SO_4 rejection under the relatively low cross-linking degree [6]. For the water permeance of TFC-X membranes with different salt solutions as feed solution, the TFC-60% membrane has a water permeance of 39.5 $L{\cdot}m^{-2}{\cdot}h^{-1}{\cdot}bar^{-1}$ with Na_2SO_4 solution as feed solution, far higher for TFC-0 membrane (15.9 $L{\cdot}m^{-2}{\cdot}h^{-1}{\cdot}bar^{-1}$). Besides, the similar trend is observed for the water permeance of the other three salts solution.

The stability of TFC NF membranes under various operating conditions is critical for their industrial application. The NF performance of TFC-0 and TFC-60% membranes was tested under different operating pressures (1–7 bar). Fig. 6a shows that there was a linear increase in pure water flux for both membranes with increasing operating pressure, while the Na_2SO_4 rejection remained essentially unchanged, indicating that the TFC-60% membrane has excellent pressure resistance. Meanwhile, the pure water flux of TFC-60% membrane was able to maintain more than 120 $L{\cdot}m^{-2}{\cdot}h^{-1}$ at low pressure (3 bar), which is meaningful to reduce energy consumption during practical application. In addition, the antifouling performance of TFC-60% and TFC-0 membranes was assessed with DI water and BSA solution (500 ppm) under 4 bar (Fig. 6b). The TFC-60% membrane displayed a higher FRR (88.6%) compared to the TFC-0 membrane. This result suggested that the TFC-60% membrane presents improved antifouling properties against pollutant owing to the increased hydrophilicity and negatively charged of membrane surface [18,43].

To further evaluate the operational stability of the membranes during the separation process, the TFC-60% and TFC-0 membranes were successively tested for 6 days with Na_2SO_4 solution (1000 ppm) (Fig. 6c). The water permeance and salt rejection remained relatively stable, demonstrating that the TFC-60% membrane has the stable structure and performance in filtration process. Moreover, we compared the separation performance of TFC-60% membrane with commercial membranes and most of the other NF membranes fabricated using similar methods in the literature (Fig. 6d and Table S3). Apparently, the TFC-60% membrane showed excellent separation performance, which presented approximately 6-fold higher pure water permeability compared to commercial membrane NF-90 meanwhile maintaining Na_2SO_4 rejection at 99.3%.

4. Conclusions

In summary, we developed a green and facile strategy for synthesizing highly permeable TFC NF membranes by using DES as an aqueous-phase additive to strengthen the diffusion control of PIP during the IP process. The DES can effectively inhibit the diffusion rate of PIP via hydrogen bonding interaction and viscosity modulation, thus regulating the surface-structure properties of the PA separation layer. When the

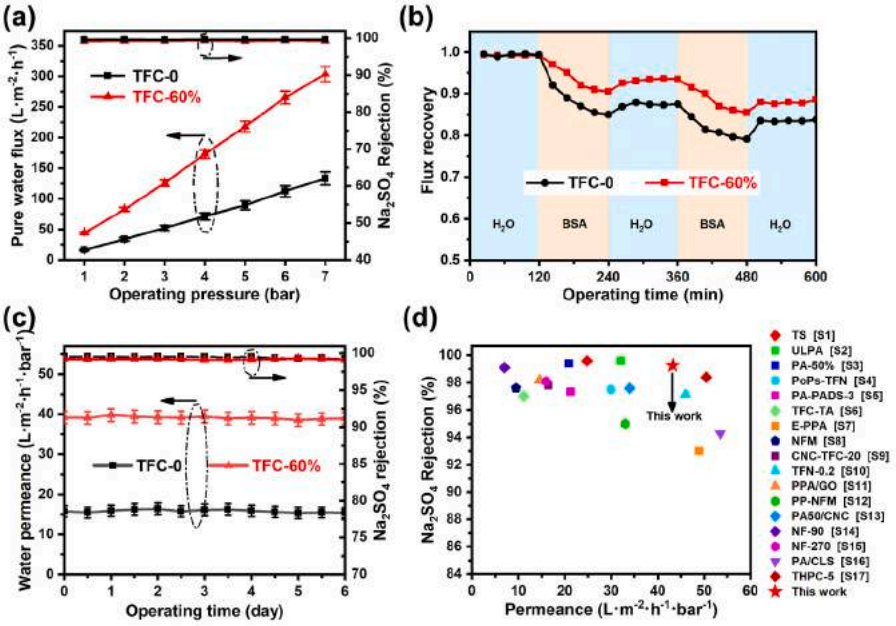

Fig. 6. (a) The pressure experiment of TFC-0 and TFC-60% membranes. (b) Antifouling properties of TFC-0 and TFC-60% membranes tested with pure water and 500 ppm BSA solution, respectively. (c) Stability performance of TFC-0 and TFC-60% membranes tested with Na_2SO_4 solution (1000 ppm) for 6 days at 4 bar. (d) Comparison of NF performance for TFC-0 and TFC-60% membranes with commercial NF membranes and other NF membranes reported in the literature.

DES concentration was 60 wt%, a thinner PA layer with optimized surface properties, which mainly included hydrophilicity, roughness and surface negative charge, was prepared on the PES substrate. The optimal TFC-60% membrane performed a favorable pure water permeance of 43.3 $L \cdot m^{-2} \cdot h^{-1} \cdot bar^{-1}$, which presented a 143% increase than the pristine TFC-0 membrane, while the Na_2SO_4 rejection remained 99.3%. Compared with the NF membranes prepared in recent literature, the excellent permeability and selectivity of TFC-60% membrane showed significant advantages. This strategy to prepare highly permeable TFC NF membranes displays great potential for Na_2SO_4 rejection. Moreover, it is considered promising to introduce electrostatic interaction or steric hindrance by changing the DES composition for the multifaceted control of amine monomer diffusion, and thus designing RO membranes with improved rejection for monovalent ions.

CRediT authorship contribution statement

Yao Fang Conceptualization, Formal analysis, Design and perform the experiments, Writing-original draft Bin Jiang: Conceptualization, Formal analysis, Design and perform the experiments, Writing-original draft. Yufan Hao, Conceptualization, Formal analysis, Writing-review & editing, Na Yang Conceptualization, Formal analysis, Writing-review & editing Longfei Zhang: Conceptualization, Formal analysis, Writing-review & editing. Congcong Zhang: Methodology, Computer simulations. Yongli Sun Formal analysis, Supervision, Validation Xiaoming Xiao: Formal analysis, Supervision, Validation. Luhong Zhang: Conceptualization, Validation, Supervision, Writing-review & editing.

Declaration of competing interest

The authors declare that they have no known competing financial interests or personal relationships that could have appeared to influence the work reported in this paper.

Data availability

No data was used for the research described in the article.

Acknowledgements

We are grateful for the financial support from National Key R&D Program of China (No. 2017B0602702). The authors also thank Shiyanjia Lab (www.shiyanjia.com) for the support of XPS test.

Appendix A. Supplementary data

Supplementary data to this article can be found online at https://doi.org/10.1016/j.memsci.2023.121689.

References

[1] C. Ji, Z. Zhai, C. Jiang, P. Hu, S. Zhao, S. Xue, Z. Yang, T. He, Q.J. Niu, Recent advances in high-performance TFC membranes: a review of the functional interlayers, Desalination 500 (2021), 114869, https://doi.org/10.1016/j.desal.2020.114869.

[2] M.M. Mekonnen, A.Y. Hoekstra, Four billion people facing severe water scarcity, Sci. Adv. 2 (2) (2016), https://doi.org/10.1126/sciadv.1500323.

[3] K. Wang, X. Wang, B. Januszewski, Y. Liu, D. Li, R. Fu, M. Elimelech, X. Huang, Tailored design of nanofiltration membranes for water treatment based on synthesis-property-performance relationships, Chem. Soc. Rev. (2021), https://doi.org/10.1039/d0cs01599g.

[4] M.Q. Seah, W.J. Lau, P.S. Goh, H.-H. Tseng, R.A. Wahab, A.F. Ismail, Progress of interfacial polymerization techniques for polyamide thin film (Nano)Composite membrane fabrication: a comprehensive review, Polymers 12 (12) (2020), https://doi.org/10.3390/polym12122817.

[5] S.-Y. Fang, P. Zhang, J.-L. Gong, L. Tang, G.-M. Zeng, B. Song, W.-C. Cao, J. Li, J. Ye, Construction of highly water-stable metal-organic framework UiO-66 thin-film composite membrane for dyes and antibiotics separation, Chem. Eng. J. 385 (2020), https://doi.org/10.1016/j.cej.2019.123400.

[6] Y. Hao, N. Yang, L. Zhang, Y. Fang, Y. Sun, B. Jiang, L. Zhang, Tailored design of highly permeable polyamide-based nanofiltration membrane via a complex-dissociation regulated interfacial polymerization, Chem. Eng. J. 452 (2023), https://doi.org/10.1016/j.cej.2022.139197.

[7] J. Li, S. Yuan, J. Zhu, B. Van der Bruggen, High-flux, antibacterial composite membranes via polydopamine-assisted PEI-TiO_2/Ag modification for dye removal, Chem. Eng. J. 373 (2019) 275–284, https://doi.org/10.1016/j.cej.2019.05.048.

[8] J. Wang, Y. Wang, J. Zhu, Y. Zhang, J. Liu, B. Van der Bruggen, Construction of TiO_2@graphene oxide incorporated antifouling nanofiltration membrane with elevated filtration performance, J. Membr. Sci. 533 (2017) 279–288, https://doi.org/10.1016/j.memsci.2017.03.040.

[9] S. Han, Z. Wang, S. Cong, J. Zhu, X. Zhang, Y. Zhang, Root-like polyamide membranes with fast water transport for high-performance nanofiltration, J. Mater. Chem. A. 8 (47) (2020), https://doi.org/10.1039/d0ta06520j.

[10] Y. Hao, Q. Li, B. He, B. Liao, X. Li, M. Hu, Y. Ji, Z. Cui, M. Younas, J. Li, An ultrahighly permeable-selective nanofiltration membrane mediated by an in situ formed interlayer, J. Mater. Chem. A. 8 (10) (2020) 5275–5283, https://doi.org/10.1039/c9ta12258c.

[11] Z. Yang, H. Guo, C.Y. Tang, The upper bound of thin-film composite (TFC) polyamide membranes for desalination, J. Membr. Sci. 590 (2019), https://doi.org/10.1016/j.memsci.2019.117297.

[12] J. Tian, B. Song, S. Gao, B. Van der Bruggen, R. Zhang, Omnifarious performance promotion of the TFC NF membrane prepared with hyperbranched polyester intervened interfacial polymerization, J. Membr. Sci. 642 (2022), https://doi.org/10.1016/j.memsci.2021.119984.

[13] Z. Tan, S. Chen, X. Peng, L. Zhang, C. Gao, Polyamide membranes with nanoscale Turing structures for water purification, Science 360 (6388) (2018) 518–521, https://doi.org/10.1126/science.aar6308.

[14] B. Yuan, C. Jiang, P. Li, H. Sun, P. Li, T. Yuan, H. Sun, Q.J. Niu, Ultrathin polyamide membrane with decreased porosity designed for outstanding water-softening performance and superior antifouling properties, ACS Appl. Mater. Interfaces 10 (49) (2018) 43057–43067, https://doi.org/10.1021/acsami.8b15883.

[15] F. Yuan, Z. Wang, X. Yu, Z. Wei, S. Li, J. Wang, S. Wang, Visualization of the formation of interfacially polymerized film by an optical contact angle measuring device, J. Phys. Chem. C 116 (21) (2012) 11496–11506, https://doi.org/10.1021/jp210209v.

[16] J.R. Werber, A. Deshmukh, M. Elimelech, The critical need for increased selectivity, not increased water permeability, for desalination membranes, Environ. Sci. Technol. Lett. 3 (4) (2016) 112–120, https://doi.org/10.1021/acs.estlett.6b00050.

[17] Z.-Y. Ma, X. Zhang, C. Liu, S.-N. Dong, J. Yang, G.-P. Wu, Z.-K. Xu, Polyamide nanofilms synthesized via controlled interfacial polymerization on a "jelly" surface, Chem. Commun. 56 (53) (2020) 7249–7252, https://doi.org/10.1039/d0cc02555k.

[18] X. Cheng, C. Lai, J. Li, W. Zhou, X. Zhu, Z. Wang, J. Ding, X. Zhang, D. Wu, H. Liang, C. Zhao, Toward enhancing desalination and heavy metal removal of TFC nanofiltration membranes: a cost-effective interface temperature-regulated interfacial polymerization, ACS Appl. Mater. Interfaces 13 (48) (2021) 57998–58010, https://doi.org/10.1021/acsami.1c17783.

[19] P. Kedchaikulrat, I.F.J. Vankelecom, K. Faungnawakij, C. Klaysom, Effects of colloidal TiO_2 and additives on the interfacial polymerization of thin film nanocomposite membranes, Colloids Surf., A 601 (2020), https://doi.org/10.1016/j.colsurfa.2020.125046.

[20] R. Cruz-Silva, S. Inukai, T. Araki, A. Morelos-Gomez, J. Ortiz-Medina, K. Takeuchi, T. Hayashi, A. Tanioka, S. Tejima, T. Noguchi, M. Terrones, M. Endo, High performance and chlorine resistant carbon nanotube/aromatic polyamide reverse osmosis nanocomposite membrane, MRS Adv 1 (20) (2016) 1469–1476, https://doi.org/10.1557/adv.2016.232.

[21] S. Bano, A. Mahmood, S.-J. Kim, K.-H. Lee, Graphene oxide modified polyamide nanofiltration membrane with improved flux and antifouling properties, J. Mater. Chem. A. 3 (5) (2015) 2065–2071, https://doi.org/10.1039/c4ta03607g.

[22] N. Zhang, X. Song, Y. Chen, B. Jiang, L. Zhang, H. Jiang, A facile and economic route assisted by trace tannic acid to construct a high-performance thin film composite NF membrane for desalination, Environ. Sci.: Water Res. Technol. 7 (5) (2021) 956–968, https://doi.org/10.1039/d1ew00071c.

[23] J. Yuan, M. Wu, H. Wu, Y. Liu, X. You, R. Zhang, Y. Su, H. Yang, J. Shen, Z. Jiang, Covalent organic framework-modulated interfacial polymerization for ultrathin desalination membranes, J. Mater. Chem. A. 7 (44) (2019) 25641–25649, https://doi.org/10.1039/c9ta08163a.

[24] Y. Gong, S. Gao, Y. Tian, Y. Zhu, W. Fang, Z. Wang, J. Jin, Thin-film nanocomposite nanofiltration membrane with an ultrathin polyamide/UIO-66-NH_2 active layer for high-performance desalination, J. Membr. Sci. 600 (2020), https://doi.org/10.1016/j.memsci.2020.117874.

[25] J. Ding, H. Wu, P. Wu, Multirole regulations of interfacial polymerization using poly(acrylic acid) for nanofiltration membrane development, ACS Appl. Mater. Interfaces (2021), https://doi.org/10.1021/acsami.1c17086.

[26] Y. Tang, L. Zhang, C. Shan, L. Xu, L. Yu, H. Gao, Enhancing the permeance and antifouling properties of thin-film composite nanofiltration membranes modified with hydrophilic capsaicin-mimic moieties, J. Membr. Sci. 610 (2020), https://doi.org/10.1016/j.memsci.2020.118233.

[27] H.R. Chae, I.C. Kim, Enhancement in permeability of piperazine-based thin-film composite membrane via surface roughening using a highly organic-soluble additive, J. Appl. Polym. Sci. 136 (36) (2019), https://doi.org/10.1002/app.47913.

[28] M. Zhang, X. You, K. Xiao, Z. Yin, J. Yuan, J. Zhao, C. Yang, R. Zhang, H. Wu, Z. Jiang, Modulating interfacial polymerization with phytate as aqueous-phase additive for highly-permselective nanofiltration membranes, J. Membr. Sci. 657 (2022), https://doi.org/10.1016/j.memsci.2022.120673.
[29] Y. Ren, J. Zhu, S. Cong, J. Wang, B. Van der Bruggen, J. Liu, Y. Zhang, High flux thin film nanocomposite membranes based on porous organic polymers for nanofiltration, J. Membr. Sci. 585 (2019) 19–28, https://doi.org/10.1016/j.memsci.2019.05.022.
[30] Y. Li, X. You, Y. Li, J. Yuan, J. Shen, R. Zhang, H. Wu, Y. Su, Z. Jiang, Graphene quantum dot engineered ultrathin loose polyamide nanofilms for high-performance nanofiltration, J. Mater. Chem. A. 8 (45) (2020) 23930–23938, https://doi.org/10.1039/d0ta09319j.
[31] Deep eutectic solvents formed between choline chloride and carboxylic acids: versatile alternatives to ionic liquids, J. Am. Chem. Soc. (2004), https://doi.org/10.1021/ja048266j.
[32] E.L. Smith, A.P. Abbott, K.S. Ryder, Deep eutectic solvents (DESs) and their applications, Chem. Rev. 114 (21) (2014) 11060–11082, https://doi.org/10.1021/cr300162p.
[33] Q. Zhang, K. De Oliveira Vigier, S. Royer, F. Jerome, Deep eutectic solvents: syntheses, properties and applications, Chem. Soc. Rev. 41 (21) (2012) 7108–7146, https://doi.org/10.1039/c2cs35178a.
[34] B. Jiang, H. Zhang, L. Zhang, N. Zhang, Z. Huang, Y. Chen, Y. Sun, X. Tantai, Novel deep eutectic solvents for highly efficient and reversible absorption of SO_2 by preorganization strategy, ACS Sustainable Chem. Eng. 7 (9) (2019) 8347–8357, https://doi.org/10.1021/acssuschemeng.8b06822.
[35] B. Jiang, C. Zhang, X. Tantai, N. Yang, L. Zhang, Y. Sun, X. Xiao, Intensification of high boiling point organic solvents on SO_2 absorption in deep eutectic solvents formed by hydroxypyridine and 1-Butyl-3-methylimidazolium chloride, J. Chem. Eng. Data 67 (11) (2022) 3435–3442, https://doi.org/10.1021/acs.jced.2c00334.
[36] D.V. Wagle, H. Zhao, G.A. Baker, Deep eutectic solvents: sustainable media for nanoscale and functional materials, Acc. Chem. Res. 47 (8) (2014) 2299–2308, https://doi.org/10.1021/ar5000488.
[37] H. Qin, Z. Song, Q. Zeng, H. Cheng, L. Chen, Z. Qi, Bifunctional imidazole-PTSA deep eutectic solvent for synthesizing long-chain ester IBIBE in reactive extraction, AIChE J. (2018), https://doi.org/10.1002/aic.16472.
[38] D. Carriazo, M.C. Serrano, M.C. Gutierrez, M.L. Ferrer, F. del Monte, Deep-eutectic solvents playing multiple roles in the synthesis of polymers and related materials, Chem. Soc. Rev. 41 (14) (2012) 4996–5014, https://doi.org/10.1039/c2cs15353j.
[39] B.B. Hansen, S. Spittle, B. Chen, D. Poe, Y. Zhang, J.M. Klein, A. Horton, L. Adhikari, T. Zelovich, B.W. Doherty, B. Gurkan, E.J. Maginn, A. Ragauskas, M. Dadmun, T.A. Zawodzinski, G.A. Baker, M.E. Tuckerman, R.F. Savinell, J. R. Sangoro, Deep eutectic solvents: a review of fundamentals and applications, Chem. Rev. 121 (3) (2021) 1232–1285, https://doi.org/10.1021/acs.chemrev.0c00385.
[40] Y. Dai, G.J. Witkamp, R. Verpoorte, Y.H. Choi, Tailoring properties of natural deep eutectic solvents with water to facilitate their applications, Food Chem. 187 (2015) 14–19, https://doi.org/10.1016/j.foodchem.2015.03.123.
[41] M. Taghizadeh, A. Taghizadeh, V. Vatanpour, M.R. Ganjali, M.R. Saeb, Deep eutectic solvents in membrane science and technology: fundamental, preparation, application, and future perspective, Sep. Purif. Technol. 258 (2021), https://doi.org/10.1016/j.seppur.2020.118015.
[42] S. Seyyed Shahabi, N. Azizi, V. Vatanpour, Tuning thin-film composite reverse osmosis membranes using deep eutectic solvents and ionic liquids toward enhanced water permeation, J. Membr. Sci. 610 (2020), https://doi.org/10.1016/j.memsci.2020.118267.
[43] N. Maalige R, S.A. Dsouza, M.M. Pereira, V. Polisetti, D. Mondal, S.K. Nataraj, Introducing deep eutectic solvents as flux boosting and surface cleaning agents for thin film composite polyamide membranes, Green Chem. 22 (8) (2020) 2381–2387, https://doi.org/10.1039/d0gc00762e.
[44] S. Sarmad, D. Nikjoo, J.-P. Mikkola, Amine functionalized deep eutectic solvent for CO_2 capture: measurements and modeling, J. Mol. Liq. 309 (2020), https://doi.org/10.1016/j.molliq.2020.113159.
[45] A. Pandey, S. Pandey, Solvatochromic probe behavior within choline chloride-based deep eutectic solvents: effect of temperature and water, J. Phys. Chem. B 118 (50) (2014) 14652–14661, https://doi.org/10.1021/jp510420h.
[46] B. Gurkan, H. Squire, E. Pentzer, Metal-free deep eutectic solvents: preparation, physical properties, and significance, J. Phys. Chem. Lett. 10 (24) (2019) 7956–7964, https://doi.org/10.1021/acs.jpclett.9b01980.
[47] S. Li, B. Gao, Y. Wang, B. Jin, Q. Yue, Z. Wang, Antibacterial thin film nanocomposite reverse osmosis membrane by doping silver phosphate loaded graphene oxide quantum dots in polyamide layer, Desalination 464 (2019) 94–104, https://doi.org/10.1016/j.desal.2019.04.029.
[48] J. Zhao, Q. Wang, J. Yang, Y. Li, Z. Liu, L. Zhang, Y. Zhao, S. Zhang, L. Chen, Comb-shaped amphiphilic triblock copolymers blend PVDF membranes overcome the permeability-selectivity trade-off for protein separation, Sep. Purif. Technol. 239 (2020), https://doi.org/10.1016/j.seppur.2020.116596.
[49] G. Wang, J. Yuan, J. Zhao, Y. Li, R. Zhang, J. Shen, X. Wang, H. Wu, A. El-Gendi, Y. Su, Z. Jiang, Anionic covalent organic framework engineered high-performance polyamide membrane for divalent anions removal, J. Membr. Sci. 650 (2022), https://doi.org/10.1016/j.memsci.2022.120451.
[50] T. El Achkar, H. Greige-Gerges, S. Fourmentin, Basics and properties of deep eutectic solvents: a review, Environ. Chem. Lett. 19 (4) (2021) 3397–3408, https://doi.org/10.1007/s10311-021-01225-8.
[51] J.H. Sonnenberg, M. Ehara, K. Toyota, R. Fukuda, J. Hasegawa, M. Ishida, T. Nakajima, Y. Honda, O. Kitao, Gaussian 09, Revision C. 01, Gaussian, Inc., Wallingford, CT, 2009.
[52] T. Lu, F. Chen, Multiwfn: a multifunctional wavefunction analyzer, J. Comput. Chem. 33 (5) (2012) 580–592, https://doi.org/10.1002/jcc.22885.
[53] V. Freger, Nanoscale heterogeneity of polyamide membranes formed by interfacial polymerization, Langmuir 19 (2003) 4791–4797.
[54] V. Freger, Kinetics of film formation by interfacial polycondensation, Langmuir 21 (2005) 1884–1894.
[55] X. Zhu, X. Tang, X. Luo, X. Cheng, D. Xu, Z. Gan, W. Wang, L. Bai, G. Li, H. Liang, Toward enhancing the separation and antifouling performance of thin-film composite nanofiltration membranes: a novel carbonate-based preoccupation strategy, J. Colloid Interface Sci. 571 (2020) 155–165, https://doi.org/10.1016/j.jcis.2020.03.044.
[56] M.J. Tang, M.L. Liu, L. Li, G.J. Su, X.Y. Yan, C. Ye, S.P. Sun, W. Xing, Solvation-amination-synergy that neutralizes interfacially polymerized membranes for ultrahigh selective nanofiltration, AIChE J. (2022), https://doi.org/10.1002/aic.17602.
[57] C.-Y. Zhu, C. Liu, J. Yang, B.-B. Guo, H.-N. Li, Z.-K. Xu, Polyamide nanofilms with linearly-tunable thickness for high performance nanofiltration, J. Membr. Sci. 627 (2021), https://doi.org/10.1016/j.memsci.2021.119142.
[58] J. Li, X. Zhu, C. Lai, F. Chen, L. Bai, X. Cheng, J. Wang, D. Wu, J. Xu, H. Liang, Triethanolamine-modulated interfacial polymerization toward microcrumpled nanofiltration membranes: performances and mechanisms, Desalination 545 (2023), https://doi.org/10.1016/j.desal.2022.116165.
[59] L. Bai, Y. Liu, N. Bossa, A. Ding, N. Ren, G. Li, H. Liang, M.R. Wiesner, Incorporation of cellulose nanocrystals (CNCs) into the polyamide layer of thin-film composite (TFC) nanofiltration membranes for enhanced separation performance and antifouling properties, Environ. Sci. Technol. 52 (19) (2018) 11178–11187, https://doi.org/10.1021/acs.est.8b04102.
[60] C.-Y. Zhu, H.-N. Li, J. Yang, J.-J. Li, J.-R. Ye, Z.-K. Xu, Vacuum-assisted diamine monomer distribution for synthesizing polyamide composite membranes by interfacial polymerization, J. Membr. Sci. 616 (2020), https://doi.org/10.1016/j.memsci.2020.118557.
[61] L. Gui, J. Dong, W. Fang, S. Zhang, K. Zhou, Y. Zhu, Y. Zhang, J. Jin, Ultrafast ion sieving from honeycomb-like polyamide membranes formed using porous protein assemblies, Nano Lett. 20 (8) (2020) 5821–5829, https://doi.org/10.1021/acs.nanolett.0c01350.
[62] S. Shao, F. Zeng, L. Long, X. Zhu, L.E. Peng, F. Wang, Z. Yang, C.Y. Tang, Nanofiltration membranes with crumpled polyamide films: a critical review on mechanisms, performances, and environmental applications, Environ. Sci. Technol. 56 (18) (2022) 12811–12827, https://doi.org/10.1021/acs.est.2c04736.
[63] Y. Lv, J. Xia, Y. Yang, Y. Chen, T. Liu, Thin-film composite membranes with mineralized nanofiber supports for highly efficient nanofiltration, Compos. Commun. 24 (2021), https://doi.org/10.1016/j.coco.2021.100695.
[64] Z.-J. Wu, H.-X. Li, P.-P. Li, Z.-L. Xu, Z.-M. Zhan, Y.-Z. Wu, Thin-film composite nanofiltration membrane modified by fulvic acid to enhance permeability and antifouling performance, Ind. Eng. Chem. Res. 61 (25) (2022) 8993–9003, https://doi.org/10.1021/acs.iecr.2c00906.
[65] N. Zhang, Z. Huang, N. Yang, L. Zhang, B. Jiang, Y. Sun, J. Ma, Nanofiltration membrane via EGCG-PEI co-deposition followed by cross-linking on microporous PTFE substrates for desalination, Sep. Purif. Technol. 232 (2020), https://doi.org/10.1016/j.seppur.2019.115964.
[66] J. Lin, W. Ye, M.-C. Baltaru, Y.P. Tang, N.J. Bernstein, P. Gao, S. Balta, M. Vlad, A. Volodin, A. Sotto, P. Luis, A.L. Zydney, B. Van der Bruggen, Tight ultrafiltration membranes for enhanced separation of dyes and Na_2SO_4 during textile wastewater treatment, J. Membr. Sci. 514 (2016) 217–228, https://doi.org/10.1016/j.memsci.2016.04.057.
[67] X. Zhu, X. Cheng, X. Luo, Y. Liu, D. Xu, X. Tang, Z. Gan, L. Yang, G. Li, H. Liang, Ultrathin thin-film composite polyamide membranes constructed on hydrophilic poly(vinyl alcohol) decorated support toward enhanced nanofiltration performance, Environ. Sci. Technol. 54 (10) (2020) 6365–6374, https://doi.org/10.1021/acs.est.9b06779.
[68] G.M. Urper-Bayram, N. Bossa, D.M. Warsinger, I. Koyuncu, M. Wiesner, Comparative impact of SiO_2 and TiO_2 nanofillers on the performance of thin-film nanocomposite membranes, J. Appl. Polym. Sci. 137 (44) (2020), https://doi.org/10.1002/app.49382.
[69] S.-J. Xu, Q. Shen, L.-H. Luo, Y.-H. Tong, Y.-Z. Wu, Z.-L. Xu, H.-Z. Zhang, Surfactants attached thin film composite (TFC) nanofiltration (NF) membrane via intermolecular interaction for heavy metals removal, J. Membr. Sci. 642 (2022), https://doi.org/10.1016/j.memsci.2021.119930.
[70] X. You, K. Xiao, H. Wu, Y. Li, R. Li, J. Yuan, R. Zhang, Z. Zhang, X. Liang, J. Shen, Z. Jiang, Electrostatic-modulated interfacial polymerization toward ultra-permselective nanofiltration membranes, iScience 24 (4) (2021), https://doi.org/10.1016/j.isci.2021.102369.